Quantifying the impact of stiffness distributions on the dynamic behaviour of railway transition zones

Jain, Avni; Marykovskiy, Yuriy ; Metrikine, Andrei V.; van Dalen, Karel N.

DOI
10.1016/j.trgeo.2024.101211

Publication date
2024

Document Version
Final published version

Published in
Transportation Geotechnics

Transportation Geotechnics 45 (2024) 101211

Contents lists available at ScienceDirect

Transportation Geotechnics

journal homepage: www.elsevier.com/locate/trgeo

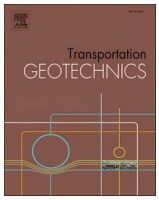

Quantifying the impact of stiffness distributions on the dynamic behaviour of railway transition zones

Avni Jain [a,*], Yuriy Marykovskiy [b], Andrei V. Metrikine [a], Karel N. van Dalen [a]

[a] TU Delft, Faculteit Civiele Techniek en Geowetenschappen, Gebouw 23, Delft 2628 CN, Netherlands
[b] ETH Zurich, Strukturmechanik und Monitoring HIL E 19.5, Stefano-Franscini-Platz 5, Zurich 8093, ZH, Switzerland

ARTICLE INFO

Keywords:
Railway transition zones
Dynamic amplifications
Material properties
Design limits
Stiffness ratios
Polynomial chaos expansion

ABSTRACT

Railway transition zones (RTZs) are regions where abrupt track stiffness changes occur that may lead to dynamic amplifications and subsequent track deterioration. The design challenges for these zones arise due to variations in material properties in both the depth (trackbed layers composed of different materials) and longitudinal directions of the track, as well as temporal variations in mechanical properties of materials due to several external factors over the operational period. This research aims to investigate the effects of these variations in material properties (i.e., of the resulting stiffness distributions in vertical and longitudinal directions) on the behaviour of RTZs, assess from this perspective the performance of a novel transition structure called the SHIELD, and establish a methodology for designing a robust solution to mitigate the dynamic amplifications in these zones. Results indicate that stiffness variations in both vertical and longitudinal directions significantly influence the dynamic behaviour of the RTZs. The study also suggests a permissible range of stiffness ratios to control the amplification of strain energy in the most critical components of RTZs, both in the initial state as well as during the operational phase (where material properties may vary over time). Moreover, the proposed methodology offers a valuable tool for the design and evaluation of RTZs and is applicable to various transition types and a broad spectrum of material properties.

1. Introduction

Railway transition zones (RTZs) are critical regions where the track stiffness changes abruptly, such as in the transition from a ballasted track to a track supported by a concrete structure. In these zones, dynamic amplification due to moving loads can lead to increased track deterioration and reduced service life [1]. In [2], a detailed literature review is presented, concerning the problem of amplified degradation in RTZs due to an abrupt stiffness variation in the foundation. Another detailed study [3] presents an overview of the existing mitigation measures (both preventive and corrective) on superstructure and substructure levels to deal with the dynamic amplifications in RTZs. Even though the influence of an abrupt increase in track stiffness in the longitudinal direction experienced by the moving load has been studied in the past [4–9], an effective design solution is lacking in practice. In addition to this, the trackbed layers (ballast, embankment and subgrade) are composed of materials with varying properties which adds to the complexity of the problem at hand [10,11]. There have been some studies [12,13] in the past on the influence of material parameters on the dynamic properties of railway transition zones. However, the current literature has no evidence of the influence of the distribution of material properties along the depth of the railway track on the behaviour of RTZs.

Even though transition structures like approach slabs [14–17] and transition wedges [18–21] are designed with an aim to achieve a gradual stiffness distribution in the longitudinal direction, it is difficult to maintain the robustness of the design of these transition structures as they are subjected to temporal variations in the mechanical properties of the materials due to environmental factors [22–24], geotechnical conditions [25], operation-induced wearing of materials etc. These factors lead to changes in the mechanical properties of the materials in terms of elastic moduli, densities and Poisson's ratios [24]. The influence of the variations in the mechanical properties of the materials on the performance of the transition structure is unknown. Therefore, a robust design solution for RTZs must take into account these variations in the above-mentioned material parameters and the related studies are lacking in the current literature.

This paper has three objectives. Firstly, the influence of the

* Corresponding author.
E-mail address: A.jain-1@tudelft.nl (A. Jain).

https://doi.org/10.1016/j.trgeo.2024.101211
Received 29 November 2023; Received in revised form 31 January 2024; Accepted 8 February 2024
Available online 15 February 2024

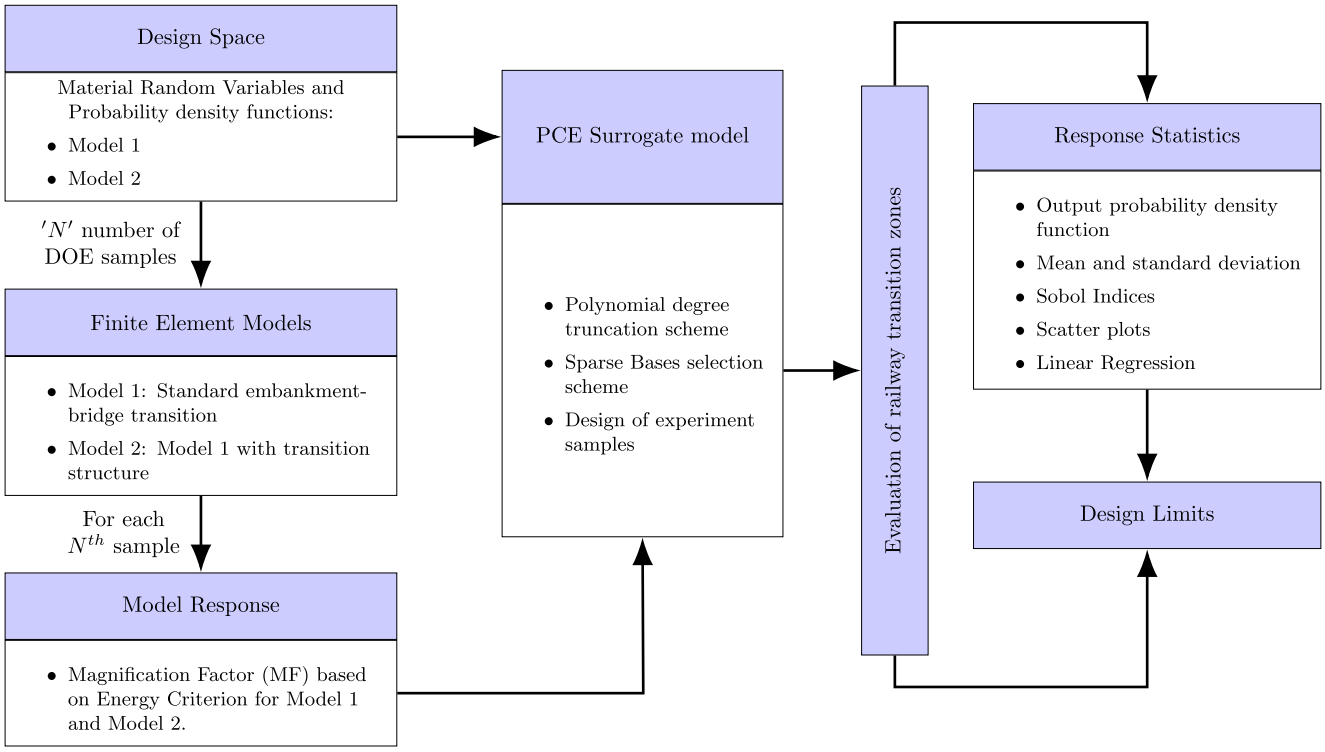

Fig. 1. Framework for evaluation of railway transition zones.

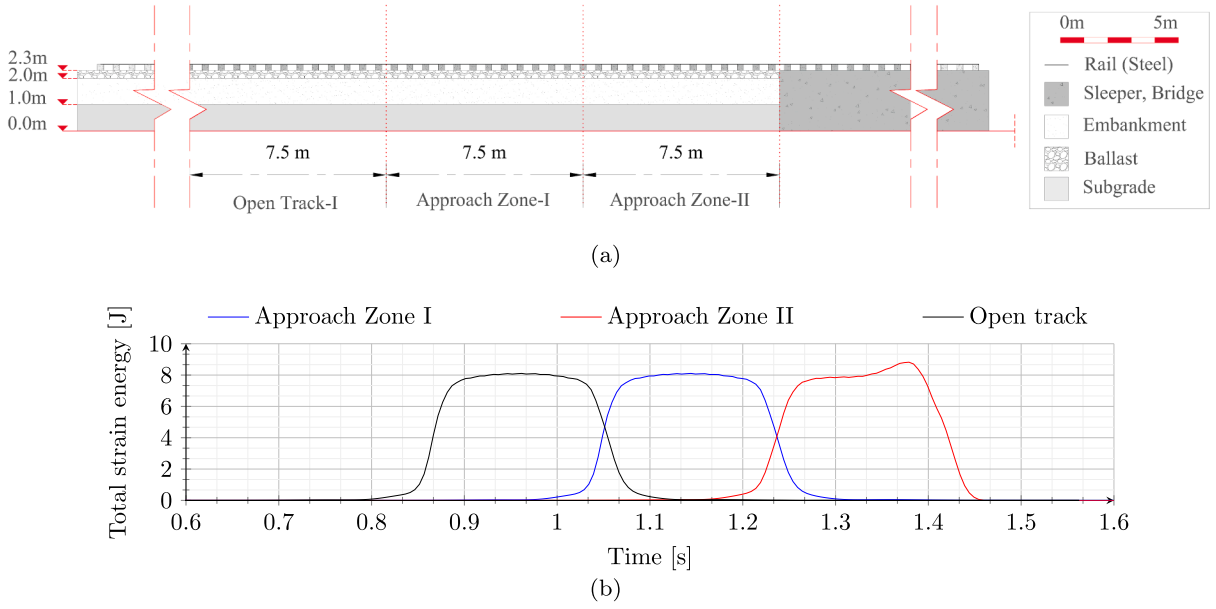

Fig. 2. (a) Geometric details of an embankment-bridge transition, (b) time history of total strain energy in OT, AZ-I and AZ-II for an embankment-bridge transition.

distribution of material properties along the depth and longitudinal directions of the track on the dynamic behaviour of a typical RTZ is investigated (Section 3.1). Secondly, the same analysis is performed for a specific transition structure, namely the safe hull-inspired energy limiting design (SHIELD) proposed by some of the authors in [26] (Section 3.2). The existing literature [18,19,2,3,27] shows that attempts have been made to mitigate the transition effects by providing a smoother stiffness transition (in the longitudinal direction) in the foundation, but it has been a challenge to quantify the permissible stiffness variation that is required to mitigate the dynamic amplifications in RTZs. Therefore, as a third objective, an appropriate set of material parameters for the design of the transition structure (SHIELD) to minimise the dynamic amplifications in RTZs is established. Based on that, the findings of this research will establish a methodology (Section 3.3) for designers to adopt an appropriate distribution of the material properties (in space and accounting for variation over the operation period) of the trackbed layers and to choose appropriate material parameters for the design of transition structures, ultimately improving their effectiveness and prolonging the service life of railway tracks in transition zones.

Table 1
Mechanical properties of the track components.

Material	Elasticity Modulus E [N/m^2]	Density ρ [kg/m^3]	Poisson's Ratio ν	Rayleigh damping α	β
Steel (rail)	21×10^{10}	7850	0.3	–	–
Concrete (sleepers)	3.5×10^{10}	2400	0.15	–	–
Ballast	1.5×10^{8}	1560	0.2	0.0439	0.0091
Sand (embankment)	8×10^{7}	1810	0.3	8.52	0.0004
Clay (subgrade)	2.55×10^{7}	1730	0.3	8.52	0.0029

Table 2
Mechanical properties of the transition structure.

Transition structure	Elastic modulus E [N/m^2]	Density ρ [kg/m^3]	Poisson's ratio ν
SHIELD	3.6 x 10^8	1900	0.2

2. Evaluation of railway transition zones: Methods

Fig. 1 shows a flow diagram of the steps/ methods adopted for the evaluation of railway transition zones using a framework for sensitivity analysis [28]. Each of the steps mentioned in the figure is discussed in detail in the following subsections.

2.1. Finite element models

The output from finite element simulations is used to create Polynomial Chaos Expansion (PCE) surrogate models. For this purpose, two finite element models are used in the present work. The first model (model 1) represents an embankment-bridge transition and the second model (model 2) incorporates a safe hull-inspired energy-limiting design of transition structure proposed by some of the authors in [26]. Both models include rail, sleepers, rail-pads, ballast, embankment and subgrade. Rails, rail-pads and sleepers have standard dimensions and material properties [8].

A 2-dimensional plane strain model (Fig. 2) of an embankment bridge transition was used with linear elastic materials. An axle load of 90 kN moving with a velocity of 144 km/hr was simulated using the DLOAD subroutine in Abaqus [29]. The details of the model used can be found in [8,26]. In accordance with the design criterion proposed in [8], the strain energy amplification in the approach zones (AZ) relative to the open track (OT) is studied for both models. In [8] authors presented a detailed analysis of kinematic response, Von Mises stress and mechanical energy (kinetic and strain energy) variations in all track components (rail, sleepers, ballast, railpad, embankment and subgrade). The strain energy was shown to be the most comprehensive quantity to evaluate the railway transition as it comprises both distortional and volumetric components of the strain energy, while Von Mises stress for instance only captures the distortional component of energy. The total strain energy used for computations in this work is the volume integral of the strain energy density (only the dynamic contribution) in the zones under study. A detailed derivation of the expression for the total strain energy can be found in [30]. It is to be noted that the strain energy amplification is studied only for the ballast layer in both models as it is the most critical layer in terms of dynamic amplifications according to [8] (model 1) and [26] (model 2).

Bridge-embankment railway transition zone (model 1): A bridge-embankment transition is one of the most critical types of railway transition zones where the stiffness change is observed on multiple levels, i.e., the interaction of all trackbed layers (ballast, embankment and subgrade) with the concrete structure. In a detailed study [8] as mentioned above, it was concluded that the amplification in the total strain energy in the trackbed layers in the proximity of the transition interface relative to the open tracks can be associated with the non-uniformity in degradation observed along the longitudinal direction of the track. However, this study was performed for a specific set of mechanical properties of trackbed layer materials (Table 1). Therefore, this paper will assess the sensitivity of the dynamic response of the RTZ to the variation in the mechanical properties of trackbed materials in vertical and longitudinal directions.

For this purpose, the mechanical parameters used to define the material of ballast, embankment and subgrade layers tabulated in Table 1 are varied as shown in Table 4. Fig. 2 shows the time history of the total strain energy in the ballast layer in open track (7.5 m) and approach zones (7.5 m), with an amplification of approximately 9% in the vicinity of the transition interface for model 1. The sensitivity of this amplification to the variation in material properties of the trackbed layers is studied in terms of magnification factor (Y_{RTZ}) defined in 2.3.

Bridge-embankment transition with SHIELD (model 2): This model is a modified version of model 1, as it has the transition structure proposed by the authors in [26]. This transition structure is placed between the ballasted track and the ballastless track to minimise the dynamic amplifications and guarantee a smooth variation of the total strain energy in the longitudinal direction. However, in [26], the design and evaluation of this transition structure were performed using a particular set of material properties of trackbed layers (Table 1). Also, the mechanical properties of the transition structure (Table 2) were chosen to provide a smooth transition from certain materials in trackbed layers to a concrete structure. Hence, in this paper, the effect of variation in the material parameters of the trackbed layers on the choice of design parameters of the transition structure will be assessed.

For this purpose, the mechanical parameters used to define the material of ballast, embankment, subgrade layers and the transition structure (TS) tabulated in Table 2 are varied as mentioned in Table 5. Fig. 3 shows the time history of the total strain energy in the ballast layer in open track (7.5 m) and approach zones (7.5 m), with no amplification of total strain energy in any of the approach zones for the set of parameters used to design this particular transition structure (model 2). It can be seen that the total strain energy in AZ-II is much lower (65%) compared to OT. However, the total strain energy in AZ-I (38% lower compared to OT) can be sensitive to the variation in the material parameters of the trackbed materials listed in Table 3. Hence, the sensitivity of this response amplification (in AZ-I compared to OT) to the variation in material properties of the trackbed layers around the TS and the efficiency of TS is assessed in terms of magnification factor (Y_{TS}) defined in Section 2.3.

2.2. Design space (input)

Design space is defined by the mechanical properties of materials (ballast, embankment, subgrade and transition structure) that are considered as random variables to account for the possible variations in their values. The mechanical parameters used to characterise the materials studied in this paper are tabulated in Table 3. The input domain of mechanical properties is defined by the probability density functions. Due to the lack of information in the current literature, uniform probability density functions denoted as $\mathscr{U}[a,b]$, were adopted for the majority of random variables. However, for the subgrade and embankment layers, preliminary investigations showed a very high sensitivity of the model response to the soil elasticity modulus. This was especially pronounced for soft soils. Adopting a fully inclusive input space of all soil types would result in soil elasticity having an overwhelming influence on the model response when compared to the effects of material properties in the remaining layers. Hence, for the purpose of this study, the distributions of soil material parameters were restricted to a single soil type (clayey soil for subgrade and sandy soil for embankment) and a

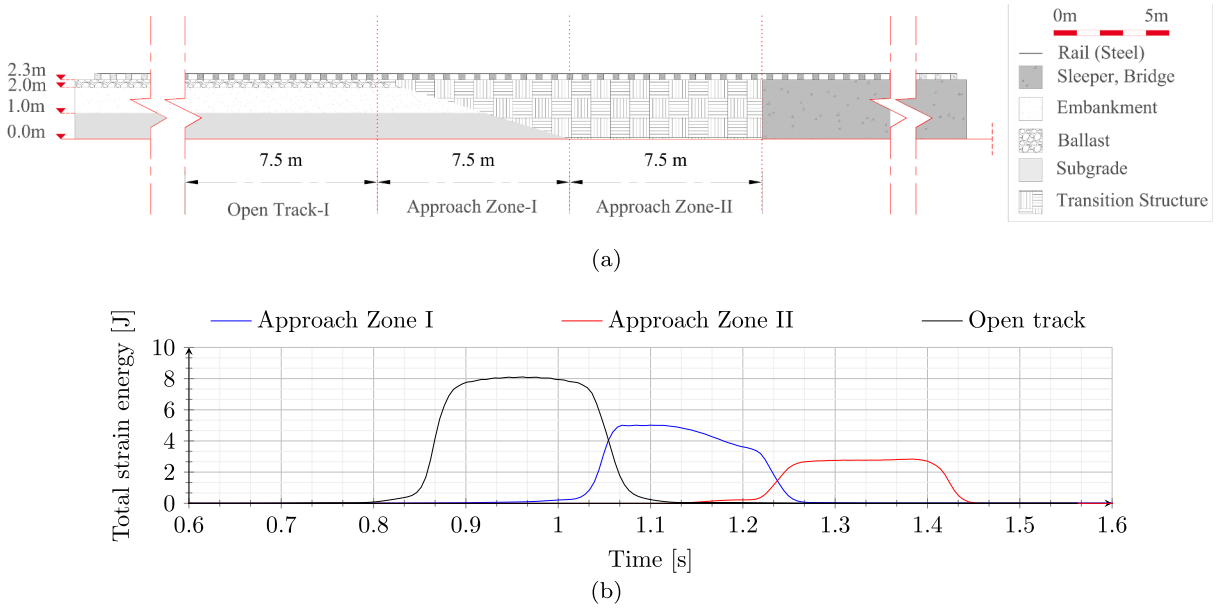

Fig. 3. (a) Geometric details of an embankment-bridge transition with SHIELD, (b) time history of total strain energy in OT, AZ-I and AZ-II for an embankment-bridge transition with SHIELD.

Table 3
Random variables defined in Table 4 and Table 5.

Layer	Elastic Modulus	Poisson's Ratio	Density
Ballast	E_b	ν_b	ρ_b
Embankment	E_e	ν_e	ρ_e
Subgrade	E_s	ν_s	ρ_s
Transition Structure	E_{TS}	ν_{TS}	ρ_{TS}

normal probability density function denoted as $\mathcal{N}(\mu, \sigma^2)$, was adopted for the elastic modulus. A detailed discussion of the possible values of the mechanical properties of the materials (adopted across the literature for modelling purposes) constituting the trackbed layers (ballast, embankment and subgrade) was presented in [31]. The data presented in [31], combined with feedback from domain and industry experts has provided a starting point in establishing the lower and upper bounds of the uniform distributions (a and b, respectively) as well as the normal probability density function moments μ and σ. It is to be noted that, the chosen input space is intentionally kept broad, in order not to restrict the analysis results to specific site conditions. Nevertheless, designers can apply the methodology outlined in this research to a specific transition zone by adopting statistical distributions that accurately reflect the site conditions. The probability density functions used in this paper, for materials forming trackbed layers (ballast, embankment and subgrade) are presented in Table 4, and for the transition structure (SHIELD) are

Table 4
Probability density functions of random variables for bridge embankment transition.

Layer	$E[\mathrm{N\,m^{-2}}]$	ν	$\rho[\mathrm{kg\,m^{-3}}]$
Ballast	$\mathcal{U}[a,b]$, a, b, E_b	$\mathcal{U}[a,b]$, a, b, ν_b	$\mathcal{U}[a,b]$, a, b, ρ_b
Embankment	$a = 1.0{\cdot}10^8$, $b = 2.5{\cdot}10^8$, $\mathcal{N}(\mu,\sigma^2)$, E_e, μ	$a = 0.15$, $b = 0.25$, $\mathcal{U}[a,b]$, a, b, ν_e	$a = 1.2{\cdot}10^3$, $b = 1.7{\cdot}10^3$, $\mathcal{U}[a,b]$, a, b, ρ_e
Subgrade	$\mu = 8.0{\cdot}10^7$, $\sigma = 5.0{\cdot}10^6$, $\mathcal{N}(\mu,\sigma^2)$, E_s, μ	$a = 0.3$, $b = 0.4$, $\mathcal{U}[a,b]$, a, b, ν_s	$a = 1.2{\cdot}10^3$, $b = 1.5{\cdot}10^3$, $\mathcal{U}[a,b]$, a, b, ρ_s
	$\mu = 2.4{\cdot}10^7$, $\sigma = 4.0{\cdot}10^6$	$a = 0.2$, $b = 0.4$	$a = 1.6{\cdot}10^3$, $b = 1.8{\cdot}10^3$

Table 5
Random variables for the transition structure of bridge embankment transition.

Layer	$E[\mathrm{N\,m^{-2}}]$	ν	$\rho[\mathrm{kg\,m^{-3}}]$
SHIELD	$\mathcal{U}[a,b]$ 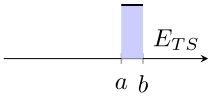	$\mathcal{U}[a,b]$ 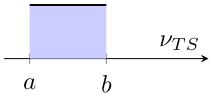	$\mathcal{U}[a,b]$ 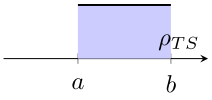
	$a = 3.5{\cdot}10^{8}$ $b = 4.0{\cdot}10^{8}$	$a = 0.15$ $b = 0.30$	$a = 1.5{\cdot}10^{3}$ $b = 2.0{\cdot}10^{3}$

reported in Table 5.

2.3. Model response

Magnification factor (MF): The amplification of the total strain energy in the approach zones relative to the open tracks is defined as the magnification factor, i.e., the ratio between the maximum total strain energy in each of these zones. The magnification factors for an embankment-bridge transition with (Y_{TS}) and without transition structure (Y_{RTZ}) are defined below.

- **MF for model 1:** Y_{RTZ} is the ratio of the maximum total strain energy in AZ-II to that in OT as shown in Fig. 2. This magnification factor is expected to be always greater than 1 due to transition effects.
- **MF for model 2:** Y_{TS} is the ratio of the maximum total strain energy in AZ-I to that in OT as seen in Fig. 3. This magnification factor is preferably smaller than 1 for an efficient design of a transition structure.

2.4. Polynomial Chaos Expansion (PCE) Surrogate Model

Given a rather wide range of possible transitions and a non-negligible computation cost of the FEM simulations, there is a need to efficiently sample the space of possible realisations. One such possibility is creating a PCE surrogate model with sparse bases. The advantages of PCE models as opposed to other surrogate model approaches are several. Firstly, these models are non-intrusive and do not require any modification to the underlying FEM simulations. Secondly, PCE models are transparent in terms of the theoretical underpinnings of their performance. Lastly, the post-processing of PCE model coefficients provides analytically computed Sobol indices, which can be used for global sensitivity analysis [32]. In the context of railway engineering the authors of [33] have recently demonstrated that PCE surrogates can be used instead of Monte Carlo simulations when modelling the response of railway embankments. Given the input space of random variables and the FEM model, a PCE surrogate model is an attractive alternative to the Monte Carlo sampling method, as it provides the benefits of faster computation, the prospect for adoption of higher fidelity, non-linear FEM models, and the capability to perform sensitivity analysis and optimization tasks more efficiently.

The PCE model in this work is built using UQlab, a framework developed at ETH Zurich [34]. This framework provides a high-level implementation of Uncertainty Quantification analysis. The details of the setup used to create PCE surrogate models employed in this work are described hereinafter.

Polynomial degree truncation scheme: It is often the case in applied science problems, that some terms in the polynomial basis have a marginal influence on the overall model response. This is known as the sparsity-of-effects principle. Based on this a hyperbolic (q-norm) polynomial degree truncation scheme [35] with $q = 0.75$ was chosen in the search of optimal basis.

Calculation of the coefficients for Sparse PCE Bases: In this study, the least angle regression algorithm [36] was used to create sparse bases and reduce the toll induced due to the high dimensionality of the input space. The minimum polynomial degree p was set to 3.

Design of Experiment (DOE) Samples: When the PCE model is built the input space is sampled at specific points, and the number of DOE samples (i.e. full FEM model evaluations) required to build the PCE surrogate model is proportional to the input space size and the degree of polynomial bases. For the standard truncation scheme, the cardinality is:

$$P = \frac{(M+p)!}{M!p!} \tag{1}$$

where M is the number of input variables and p is the polynomial expansion degree. In the case of least-square minimization, if the number of samples n is smaller than P, it leads to an underdetermined system, while $n = P$ may lead to overfitting. As a rule of thumb,

$$n = k{\cdot}P \tag{2}$$

with $k = 2 \sim 3$. By adopting the hyperbolic truncation scheme and the least angle regression algorithm, the number of evaluations can be significantly reduced. In fact, the common practice is to set the initial number of full model evaluations to $n = 10{\cdot}M$. Leave One Out (LOO) error can serve as an indicator of the surrogate model accuracy when selecting the minimum polynomial degree and the number of DOE samples. For the present analysis, 100 FEM model evaluation resulted in ϵ_{LOO} of the order 10^{-3} for both model 1 and model 2. Generally, $\epsilon_{LOO} \leq 10^{-2}$ is sufficient for the purpose of global sensitivity analysis.

2.5. Response Statistics

The following results will be presented and analyzed in this paper (Section 3):

1. Probability density function (PDF): A log-normal distribution provided a good fit for the surrogate model responses. The log-normal distribution was chosen as opposed to a Gaussian, as model responses, represented by magnification factors, are always positive. The PDF of a log-normal distribution can be expressed as follows:

$$\psi(x,s,l,s_c) = \frac{1}{(x-l){\cdot}s\sqrt{2\pi}}{\cdot}\exp\left(\frac{-\ln^2(x-l)+\ln^2(s_c)}{2s^2}\right) \tag{3}$$

   where x is the random variable and the shape (s), location (l), and scale (s_c) parameters are used to specify the particular log-normal distribution fitting the data.
2. Mean (μ) and standard deviation (σ): The upper and lower limits are marked in probability density function graphs as per the empirical rule in statistics to include 90% data. In mathematical notation, these facts can be expressed as follows, where Pr is the probability function [37,38], X is an observation from a normally distributed random variable according to Eq. (4)

$$\Pr(\mu - 1.6{\cdot}\sigma < \mathrm{X} < \mu + 1.6{\cdot}\sigma) = 90\% \tag{4}$$

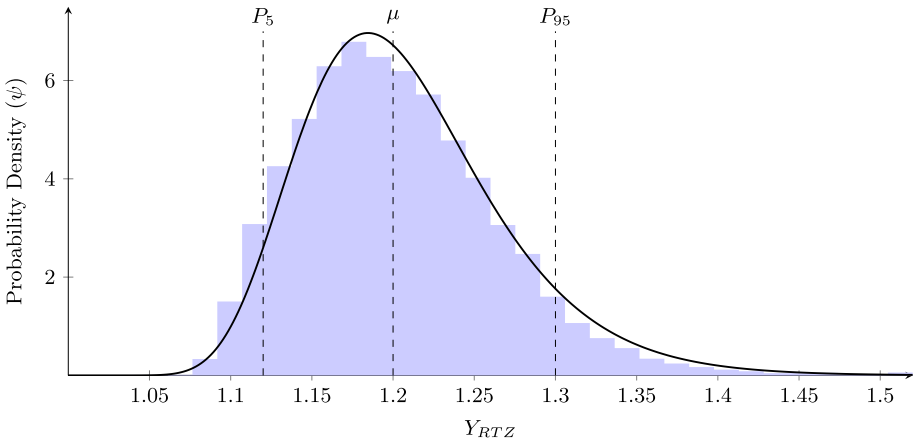

Fig. 4. Probability density distribution of the amplification factor.

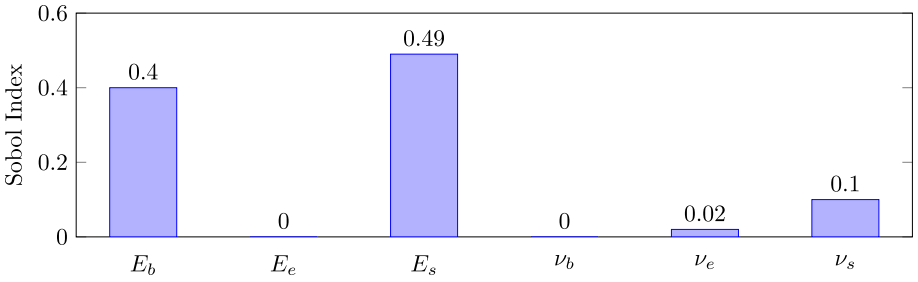

Fig. 5. Total Sobol indices for input space parameters in model 1.

3. Sobol indices: Sobol indices are used in sensitivity analysis to identify which variables have the greatest impact on the output of a system. They are calculated by partitioning the variance of the output into contributions from individual variables and combinations of variables. The first-order Sobol index measures the contribution of individual variables to the variance, while the total-effect Sobol index measures the contribution of the individual variables and all of their interactions to the variance. A comparison of Sobol indices of the most influential parameters is done for model 1 and model 2.
4. Scatter plots: The scatter plots are studied mainly for two types of parameters. Firstly, the parameters with the most significant contribution (in terms of Sobol indices) to the critical values of the magnification factor are investigated in detail. Secondly, as discussed in Section 1, even though the effects of stiffness variation in the longitudinal direction on the dynamic amplifications in RTZs is well known, there is no investigation on the influence of stiffness variation in the vertical direction on the dynamic behaviour of RTZs. Therefore, the influence of the stiffness ratios on the magnification factor will be analysed for all the cases under study. All scatter plots will be evaluated in terms of the quantities discussed below.
   - R-squared (strength): The coefficient of determination, also known as R-squared, is a statistical measure that represents the proportion of the variance for a dependent variable that's explained by an independent variable or variables in a regression model.
   - Spearman correlation coefficient: This coefficient is a measure of the strength and direction of the monotonic relationship between two variables. It measures how well the relationship between two variables can be described by a monotonic function, such as a straight line or a curve. Spearman correlation coefficient ranges from -1 to $+1$, where a value of -1 indicates a perfectly negative correlation, 0 indicates no correlation, and $+1$ indicates a perfectly positive correlation.
   - Linear regression line: This is a statistical method to find the best-fitting line through the data points in a scatter plot. This line can be used to predict the values of a variable based on the value of another variable.

3. Evaluation of railway transition zones: Results and Discussion

An initial analysis was performed to compare the Sobol indices of the parameters under study to highlight the most influential parameters. It was observed that the densities of materials had no influence on the dynamic response of the system for both the models studied in this work. Therefore, in this section, the influence of elastic moduli and Poisson's ratios of different materials on the magnification factor is investigated, both for a typical transition zone without transition structure (Section 3.1) and with transition structure (Section 3.2). In addition, design limits are formulated for the latter to ensure that dynamic amplifications are avoided (Section 3.3).

3.1. Model 1

In this section, the results are presented for model 1 to study the dependence of the magnification factor (Y_{RTZ}) on the variation in the mechanical properties of the materials. It is to be noted that even though the variation in material properties is implemented in the vertical direction keeping the properties of the concrete bridge constant, there is a stiffness variation in both vertical and longitudinal directions (and the latter is affected as the stiffness of the layers in vertical direction, changes as per Table 4).

Probability density function (PDF): Fig. 4 shows the probability density of the magnification factor Y_{RTZ} for the case without transition structure. It can be seen that 90% of the data belongs to the values of Y_{RTZ} lying between 1.12 and 1.3. This implies that for all combinations of parameters under study, the amplification in strain energy is approximately 12% to 30%. The mean (μ) and standard deviation (σ) of the distribution are 1.2 and 0.06, respectively. The probability density function of a log-

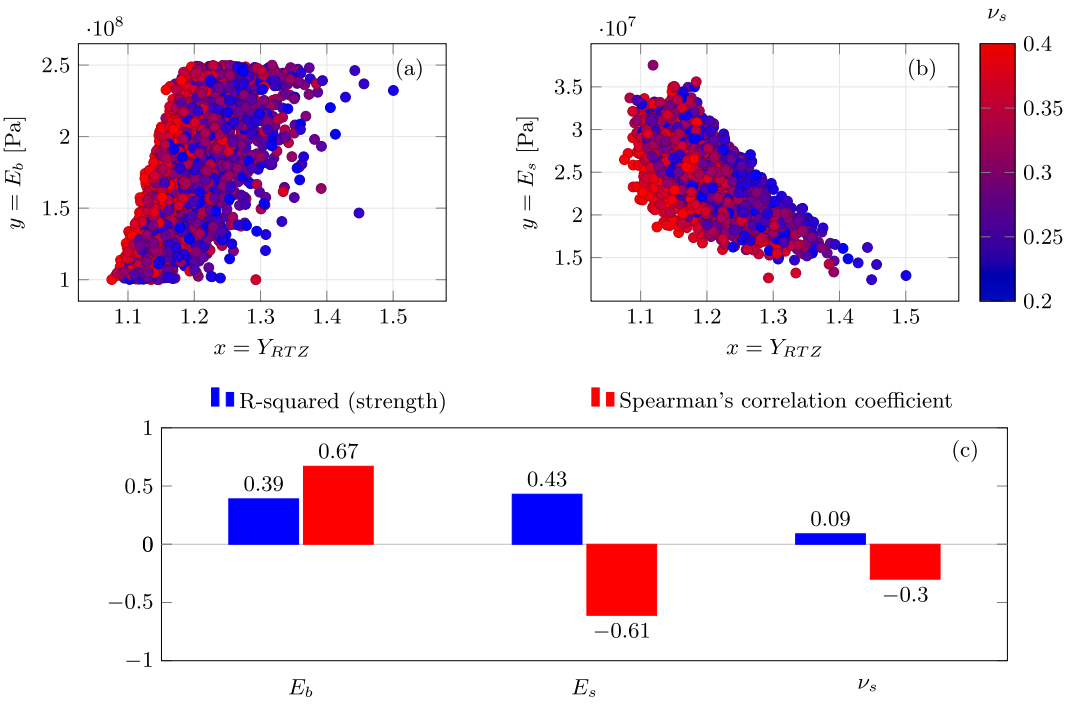

Fig. 6. Scatter plot of (a) E_b and (b) E_s for model 1. (c) Bar chart showing the comparison of the R-squared (strength) and Spearman's correlation coefficient for the scatter plots.

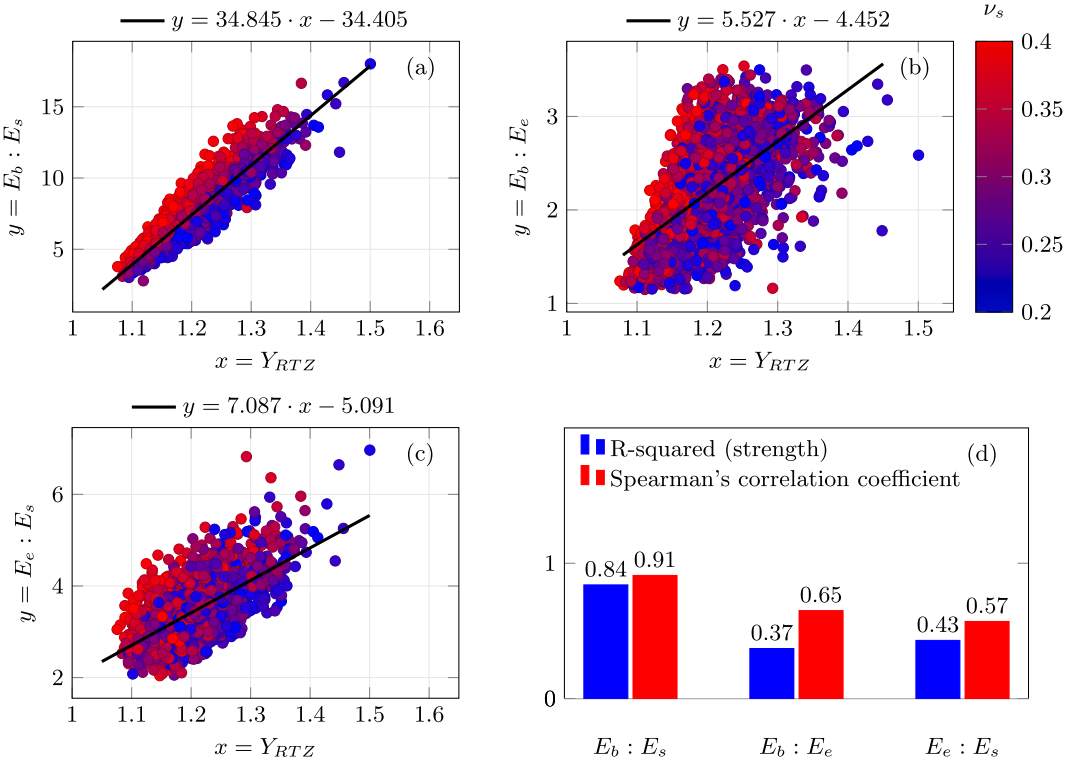

Fig. 7. Scatter plot of the ratios (a) $E_b : E_S$, (b) $E_b : E_e$ and (c)$E_e : E_s$ for model 1. (d) Bar chart showing the comparison of the R-squared (strength) and Spearman's correlation coefficient for the scatter plots.

normal distribution (Eq. 3) can describe the obtained probability density (shown in Fig. 4) when the following choices are made (Y_{RTZ} is the random variable): s is 0.27, l is 0.98 and s_c is 0.22.

Sobol indices: Fig. 5 shows the Sobol indices for all the parameters (E_b, E_e, E_s, ν_b, ν_e, ν_s) under study. It can be clearly seen that the elasticity modulus for ballast (E_b) and subgrade (E_s) are the most influential parameters. While the Poisson's ratio of the ballast and embankment layers shows no influence on Y_{RTZ}, the Poisson's ratio for the subgrade layer (ν_s) has a marginal influence on the magnification factor. Hence, in the following sections mainly E_b, E_s and ν_s will be investigated in detail. In

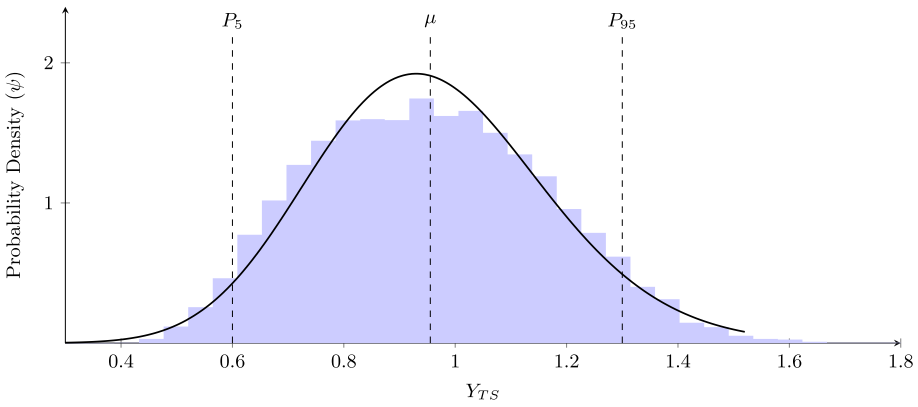

Fig. 8. Probability density distribution of the amplification factor.

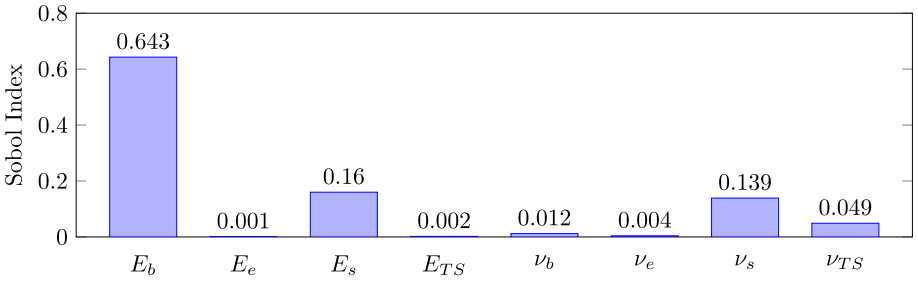

Fig. 9. Total Sobol indices for input space parameters in model 2.

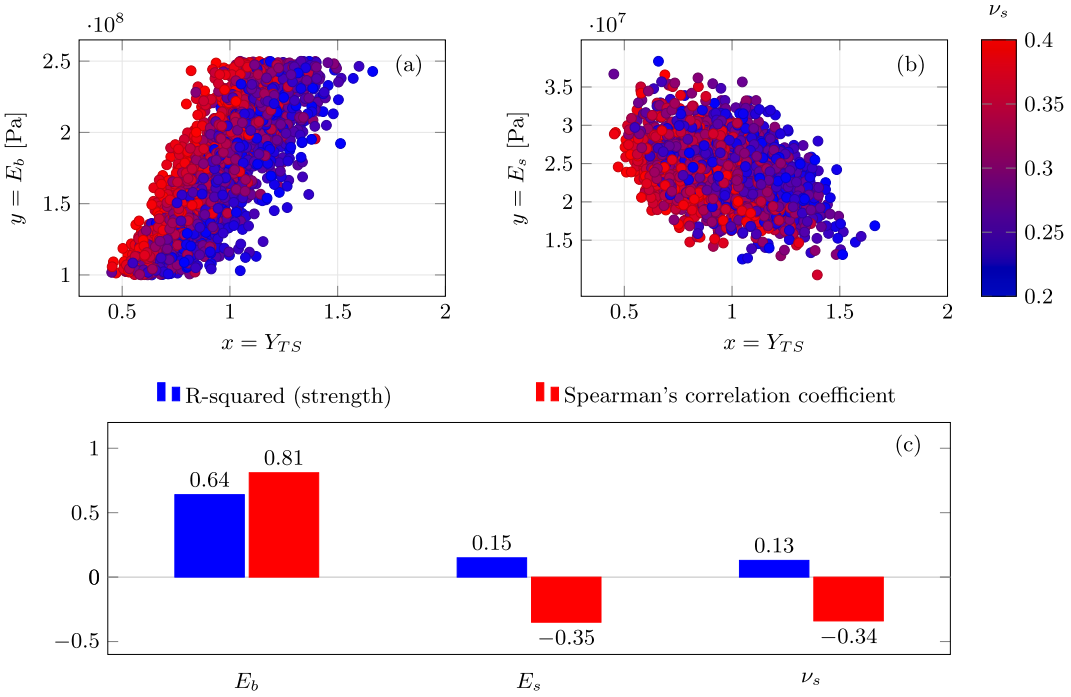

Fig. 10. Scatter plot of (a) E_b and (b) E_s for model 2. (c) Bar chart showing the comparison of the R-squared (strength) and Spearman's correlation coefficient for the scatter plots.

addition to these parameters, as discussed in Section 2.5, the ratios of elastic moduli of the trackbed layers will be studied too.

Scatter of parameters (E_b, E_s): In the previous paragraph, Sobol indices (see Fig. 5 show that E_b and E_s were the most influential parameters and ν_s was marginally influential. Therefore, in this paragraph, only these three parameters are investigated. Fig. 6 presents the scatter plots of E_b (a) and E_s (b) with Y_{RTZ}, showing the influence of ν_s by means of colour gradient. Fig. 6(c) shows a detailed investigation of these scatter plots in terms of strength and correlation coefficient. On one hand, a strong correlation of Y_{RTZ} is observed with both E_b (positive) and E_s (negative). On the other hand, ν_s shows some effect on Y_{RTZ} only for very low values (smaller than 0.3). Hence, the scatter plot of ν_s was not

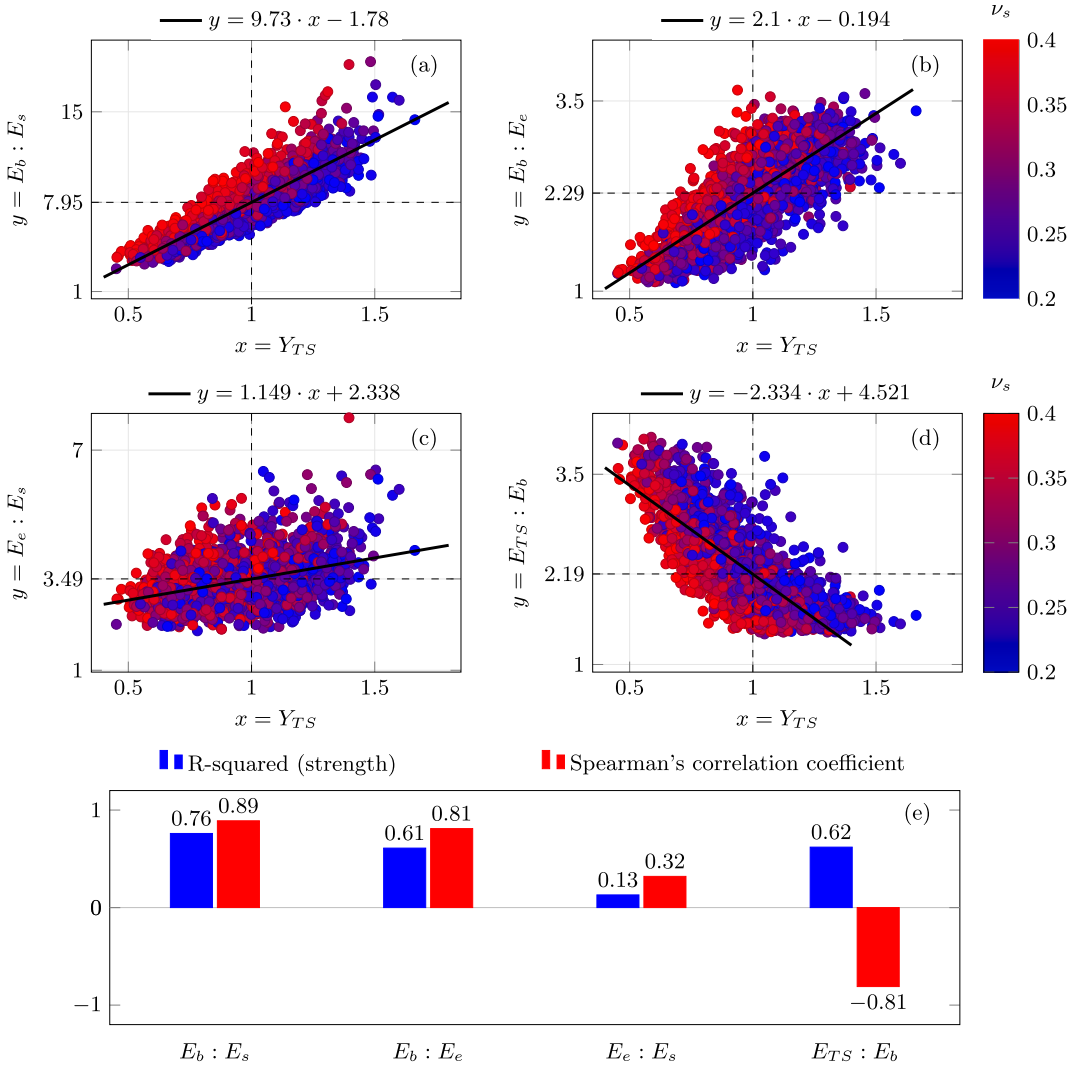

Fig. 11. Scatter plot of the ratios (a) $E_b : E_S$, (b) $E_b : E_e$, (c)$E_e : E_s$ and (d) $E_{TS} : E_b$ for model 2. (e) Bar chart showing the comparison of the R-squared (strength) and Spearman's correlation coefficient for the scatter plots.

Table 6
Design limits for ballast, embankment, subgrade and transition structure.

Layer	Design Limits	Distribution
Ballast (E_b)	$E_b > 150$ [MPa] $E_b < 250$ [MPa]	$E_b \sim \mathscr{U}[a,b]$ $a = 150$ [MPa] $b = 250$ [MPa]
Embankment (E_e)	$E_e > \frac{1}{2.3}E_b$ $E_e < 3.5 \cdot E_s$	$E_e = E_b\left(\frac{1}{2.3} + R_e\left(\frac{3.5}{R_s} - \frac{1}{2.3}\right)\right)$ $R_e \sim \mathscr{U}[a,b]$ $a = 0, b = 1$
Subgrade (E_s)	$E_s > \frac{1}{8}E_b$ $E_s < \frac{1}{2}E_b$	$E_s = R_s \cdot E_b$ $R_s \sim \mathscr{U}[a,b]$ $a = \frac{1}{8}, b = \frac{1}{2}$
Transition Structure (E_{TS})	$E_{TS} > 2 \cdot E_b$ $E_{TS} < 3 \cdot E_b$	$E_{TS} = R_{TS} \cdot E_b$ $R_{TS} \sim \mathscr{U}[a,b]$ $a = 2, b = 3$

studied as the Spearman correlation coefficient and the R-squared coefficient of the scatter plot of ν_s is negligible compared to E_b and E_s.

Scatter of ratios ($E_b : E_s$, $E_b : E_e$, $E_e : E_s$): Fig. 7 presents the scatter plots of the ratios $E_b : E_s$ (a), $E_b : E_e$ (b) and $E_e : E_s$ (c) with Y_{RTZ}, showing the influence of ν_s by means of colour gradient. A strong positive correlation is observed between $E_b : E_s$ and Y_{RTZ} in the scatter plots with the highest R-squared strength (0.84) and Spearman's correlation coefficient (0.91) compared to $E_b : E_e$ and $E_e : E_s$ as shown in Fig. 7 (d). In addition to these, the slope of the regression line for $E_b : E_s$ is significantly large, demonstrating a strong dependence of Y_{RTZ} on $E_b : E_s$ confirming the results shown in Fig. 7(d).

In summary, the most influential parameters that contribute to the amplification of the dynamic response in RTZs are the elastic moduli of the ballast (E_b) and subgrade (E_s). Additionally, the Poisson's ratio of the subgrade affects the response amplification to some extent only when the magnitude is less than 0.3. However, as seen in Fig. 7(d), when compared to the influence of the stiffness ratios, the contribution of the individual parameters is surpassed by all the ratios under study in terms of both strength and correlation factor. Furthermore, the $E_b : E_s$ ratio dominates the comparison of all parameters and ratios under study, implying that a small change in this ratio can result in a large amplification of the dynamic response due to the reasons explained below. For completeness, it is noted that the vertical stiffness ratios do not only matter because they influence the stiffness ratio in the horizontal direction of the track, but also influence the magnification factor (Y_{RTZ}) even if the stiffness ratio in the horizontal direction of the track does not change (as shown in [26]).

The distribution of energy in a system (like the one under study in model 1) composed of three layers of different materials, where the load moves over a foundation of decreasing stiffness along the vertical di-

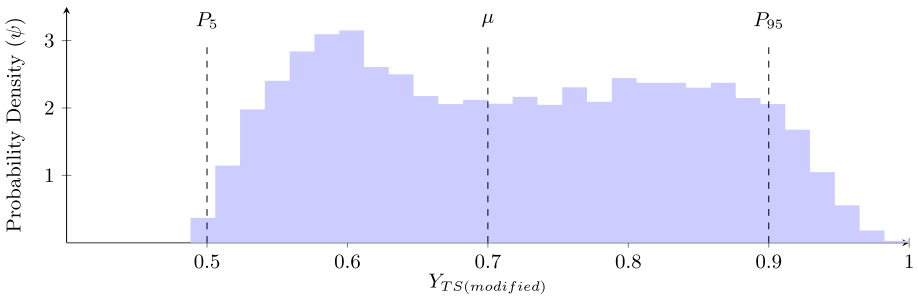

Fig. 12. Probability density distribution of the magnification factor.

rection (from stiffer to softer layers) and abruptly changing stiffness in the longitudinal direction, can be explained as follows:

1. Energy distribution in the open trackresponse: The energy distribution over the different layers (in vertical direction) in the deformation field that moves with the load (in the open track) depends on the stiffness ratios. Generally, the stiffer a specific layer, the more energy gets concentrated in it. This can lead to a non-uniform energy distribution over the layers and energy can thus be concentrated in a relatively stiff layer (e.g., the ballast), which can become problematic in transition zones (see point 3).
2. Reflection and transmission of waves: Generally, when a wave encounters a boundary between two different materials, some of the energy carried by the wave is reflected back into the original material, and some is transmitted into the new material [39]. The proportion of energy that is reflected or transmitted depends on the difference in properties between the two materials; generally, the larger the contrast in stiffness (or more specifically, the impedance), the stronger the reflection. In the case under study, the ratios of stiffness ($E_b : E_s$, $E_b : E_e$, $E_e : E_s$) between two consecutive layers along the depth play a significant role.
3. Energy distribution in the RTZ: Amplifications in the response of the different track components and trackbed layers are the result of energy concentrations. As stated, large stiffness ratios will lead to energy concentrations in the open track response that approaches a RTZ (see point 1). The waves that are generated when the load enters and crosses the RTZ will not only be most energetic in the stiffer layers but most of the energy will also be trapped in these layers (in the form of guided waves [39,40]) due to the large stiffness ratios (see point 2). This can lead to significant energy concentrations in stiff components.

The above-mentioned points explain the distribution of energy in the system under study and the actual behaviour therefore depends on the difference in stiffness between the layers, and how the stiffness changes from one layer to the other layer (gradually or abruptly). Hence, in order to obtain a uniform energy distribution along the depth of the trackbed layers, it is important to keep the ratios mentioned above under check and within permissible values such that the energy level in the stiffest layer (ballast) that is typically most prone to degradation does not exceed the critical values. In conclusion, a smoother stiffness variation in both vertical and longitudinal directions can ensure an uninterrupted energy flow and no trapping or concentration of energy at any particular location of the system. In all situations, energy concentrations should be avoided.

3.2. Model 2

In this section the results are presented for model 2, to study the influence of the variation in the mechanical properties of the materials on the strain energy amplification in the vicinity of the transition structure. The bounds of the material parameters for the trackbed layers (ballast, embankment and subgrade) are exactly the same as case 1 with an addition of transition-structure material parameters as mentioned in Section 2.2.

Probability density function: Fig. 8 shows the probability density of the magnification factor Y_{TS} for model 2. It can be seen that 90% of the data belongs to the values of Y_{TS} lying between 0.6 and 1.3. The mean and standard deviation of the distribution are 0.9 and 0.2 respectively. It is worth noting that by just introducing a transition structure, the mean is reduced from 1.2 (model 1) to 0.9 (model 2). The probability density function of a log-normal distribution shown in Fig. 8 can be obtained by using Eq. 3, where Y_{TS} is the random variable, s is 0.097, l is -1.2 and s_c is 2.15.

Sobol indices: Fig. 9 shows the Sobol indices for all the parameters (E_b, E_e, E_s, E_{TS}, ν_b, ν_e, ν_s, ν_{TS}) under study. It can be clearly seen that the elasticity modulus for ballast (E_b) is the most influential parameter. Other than E_b, material parameters associated with subgrade (E_s and ν_s) show a minor contribution to the amplification factor (Y_{TS}). Hence, in the following sections mainly E_b, E_s and ν_s will be investigated in detail similar to Section 3.1. In addition to these parameters, similar to model 1, the ratios of elastic moduli of trackbed layers and transition structure will be studied too. The ratios $E_b : E_s$, $E_b : E_e$ and $E_e : E_s$ will be investigated with an additional ratio ($E_{TS} : E_b$) representing the stiffness variation in the longitudinal direction of the track. It is to be noted that the stiffness ratio in the longitudinal direction is studied for model 2 but not for model 1 as the material properties of the transition structure are varied (in model 2) according to Table 6 but the properties of the concrete bridge are kept constant in both model 1 and model 2.

Scatter of parameters (E_b and E_s): Fig. 10 presents the scatter plots of E_b (a) and E_s (b) with Y_{TS}, showing the influence of ν_s by means of colour gradient. Fig. 10(c) shows a detailed investigation of these scatter plots in terms of strength and Spearman's correlation coefficient associated with these scatter plots. Similar to model 1, a strong correlation is seen between E_b and Y_{TS}. In addition to these, a comparatively small influence of E_s is seen on Y_{TS}. Moreover, similar to model 1 ν_s is influential only for values smaller than 0.3.

Scatter of ratios ($E_b : E_s$, $E_b : E_e$, $E_e : E_s$, $E_{TS} : E_b$): Fig. 11 presents the scatter plots of the ratios $E_b : E_s$ (a), $E_b : E_e$ (b), $E_e : E_s$ (c) and $E_{TS} : E_b$ (d) with Y_{TS}, showing the influence of ν_s by means of color gradient. A strong positive correlation of Y_{TS} is observed with $E_b : E_s$ (0.89) and $E_b : E_e$ (0.80) as shown in Fig. 11(e). In addition to this, a strong negative correlation of Y_{TS} is observed with $E_{TS} : E_b$ (0.81). Fig. 11 also shows the regression line for each scatter plot intersecting with the vertical line at Y_{TS}=1 (critical value of Y_{TS}) marking the critical allowable values of the ratios under study on the vertical axis of each of the plots.

The allowable ranges of the stiffness ratios identified based on observations discussed above and shown in Fig. 11 can be summarised as follows:

- $E_b : E_s$ must be kept smaller than 8
- $E_b : E_e$ must be kept smaller than 2.3
- $E_e : E_s$ must be kept smaller than 3.5
- $E_{TS} : E_b$ must be kept larger than 2.2

The ratios of elastic moduli of materials of trackbed layers ($E_b : E_s$, $E_b : E_e$ and $E_e : E_s$) must be controlled for the same reasons as discussed in the previous section concerning model 1. As for the ratio $E_{TS} : E_b$, which represents a stiffness change in the longitudinal direction of the track, it is expected to be within certain limits as this ratio ($E_{TS} : E_b$) being too small implies that the transition structure is not stiff enough compared to ballast in order to provide a smooth transition to the bridge. However, if this ratio is too high, it might lead to similar transition effects as in the case without any transition structure.

3.3. Design Limits

This section summarises the conclusions obtained from model 1 and model 2 and in the end suggests a permissible range of the stiffness ratios to minimise the dynamic amplifications in the railway transition zones. The mean and standard deviation of the two cases under study provide useful insight into the behaviour of the two systems, particularly the central tendency (average dynamic amplification) and variability (consistency of the dynamic amplification).

System without transition structure (model 1): With a mean of 1.2 and a standard deviation of 0.06, this system shows a higher average dynamic amplification (mean in Fig. 4) compared to model 2. The low standard deviation indicates that the amplification values are quite consistent - they tend to be close to the average value of 1.2. This could suggest that without a transition structure, the railway track consistently experiences a higher level of dynamic amplification and these dynamic amplifications are sensitive to variations in the mechanical properties of the materials in the system.

System with transition structure (model 2): With a mean of 0.9 and a standard deviation of 0.2, this system shows a lower average dynamic amplification (mean in Fig. 8) compared to model 1, suggesting that the transition structures are effective in reducing the average dynamic amplification. However, the larger standard deviation indicates that the dynamic amplification values are more spread out and they vary more around the average. This could suggest that the effectiveness of the transition structures is not assured for all scenarios, reducing dynamic amplification significantly in some but less so in others. This is due to no active control over the relative stiffness or stiffness ratios when the materials present in the system are subjected to variations, leading to a non-uniform energy distribution within the system. This can be controlled by designing the trackbed layers around transition zones such that the relative stiffness of the materials in vertical and longitudinal directions stay within the ranges suggested in Section 3.2.

As mentioned in previous paragraphs, the designers must choose the material properties of the trackbed layers and the transition structure such that even though there is a variation in the mechanical properties of the materials, the stiffness ratios are always kept in the permissible range. Therefore, based on the permissible ranges of these ratios proposed in Section 3.2, the mechanical properties of the materials are varied such that stiffness ratios R_e, R_s and R_{TS} are restricted (see Table 6) and the design space for model 2 is modified such that the stiffness ratios are bounded (similar to parameters in Table 4 and Table 5) with the aim to verify if the magnification factor is indeed minimized. The new design space is defined as described below.

The Poisson's ratios (ν_b, ν_e and ν_{TS}) are fixed for all the materials as they showed no significant influence on Y_{TS}. ν_s is kept constant at 0.3 as lower values are usually expected for fully unsaturated clayey soil which is unlikely to be found in reality. The elastic moduli of the materials for the trackbed layers and transition structure are defined as random variables with their relative distributions reported in Table 6.

Fig. 12 shows the probability density of the magnification factor Y_{TS} for the case with a transition structure (SHIELD) and the material parameters bounded as defined in Table 6. In this case, the PDF resembles that of a uniform distribution, as opposed to a log-normal one. It can be seen that 90% of the data belongs to the values of Y_{TS} lying between 0.5 and 0.9. The mean and standard deviation of the distribution are 0.7 and 0.12 respectively. The mean is reduced from 0.9 to 0.7 when compared to case 2. Most importantly, all the values lie below the critical value (Y_{TS}=1) which is expected and desired for minimising the degradation in RTZs.

4. Conclusion

In this paper, a methodology to adopt an appropriate distribution (in space and accounting for the variation over the operation period) of the material properties in a railway transition zone is presented. The results of the study presented in this paper can be concluded as follows.

The behaviour of a standard embankment-bridge transition (model 1) subjected to variations in mechanical properties of the trackbed materials (ballast, embankment and subgrade) was investigated. While it is known that the stiffness variation in the longitudinal direction leads to dynamic amplification when the transition is subject to a moving load, this work has demonstrated that the stiffness variation in the vertical direction also significantly influences the dynamic behaviour of railway transition zones.

The efficiency of a recently proposed transition structure (SHIELD) was evaluated (model 2) when subjected to variations in the mechanical properties of the trackbed materials. Similar to model 1, the results for model 2 show that the stiffness ratios in longitudinal and vertical directions are the most influential parameters in determining the strain energy amplifications (strain energy is correlated to degradation) in railway transition zones. Moreover, for the system under study and the bounds adopted for the variation of material properties of the trackbed layers and SHIELD, a permissible range of design ratios is suggested to control the amplification of strain energy in all components of railway transition zones.

Lastly, based on the allowable range of stiffness ratios obtained from model 2, new bounds for the material properties of the ballast, embankment, subgrade and transition structure were formulated to ensure no amplification of strain energy. It was demonstrated that it is possible to mitigate the strain energy amplifications if the stiffness ratios in vertical and longitudinal directions are kept in check. We note that the stiffness ratios should be respected both in the design of the transition zone and structures (initial state) as well as during the operational phase (where the properties may vary over time).

The methodology adopted in this work to evaluate the behaviour of railway transition zones with or without a transition structure both in the initial design phase and when subjected to variation in material properties, and to establish the design limits on the material properties of the trackbed layers and the transition structure can be generalised for any type of transition zone and a wide set of material properties.

Declaration of Competing Interest

The authors declare that they have no known competing financial interests or personal relationships that could have appeared to influence the work reported in this paper.

Data availability

Data will be made available on request.

Acknowledgements

This research is supported by the Dutch Technology Foundation TTW (Project 15968), a part of the Netherlands Organisation for Scientific Research (NWO), and which is partly funded by the Ministry of Economic Affairs.

References

[1] Namura A, Suzuki T. Evaluation of countermeasures against differential settlement at track transitions. Quart Rep RTRI 2007;48(3):176–82. https://doi.org/10.2219/rtriqr.48.176.

[2] Indraratna B, Sajjad MB, Ngo T, Correia AG, Kelly R. Improved performance of ballasted tracks at transition zones: A review of experimental and modelling approaches. Transport Geotech 2019;21:100260. https://doi.org/10.1016/j.trgeo.2019.100260.

[3] Sañudo R, dell'Olio L, Casado J, Carrascal I, Diego S. Track transitions in railways: A review. Constr Build Mater 2016;112:140–57. https://doi.org/10.1016/j.conbuildmat.2016.02.084.

[4] Coelho BZ, Hicks MA. Numerical analysis of railway transition zones in soft soil. Proc Inst Mech Eng, Part F: J Rail Rapid Transit 2015;230(6):1601–13. https://doi.org/10.1177/0954409715605864.

[5] Selig ET, Li D. Track modulus: Its meaning and factors influencing it. Transport Res Rec. http://onlinepubs.trb.org/Onlinepubs/trr/1994/1470/1470-006.pdf.

[6] Fortunato E, Paixão A, Calçada R. Railway track transition zones: Design, construction, monitoring and numerical modelling. Int J Railway Technol 2013;2(4):33–58. https://doi.org/10.4203/ijrt.2.4.3.

[7] Zakeri JA, Xia H. Sensitivity analysis of track parameters on train-track dynamic interaction. J Mech Sci Technol 2008;22(7):1299–304. https://doi.org/10.1007/s12206-008-0316-x.

[8] Jain A, Metrikine AV, Steenbergen MJMM, van Dalen KN. Design of railway transition zones: a novel energy-based criterion (2023). arXiv:2310.07956. doi: https://doi.org/10.48550/arXiv.2310.07956. URL: https://arxiv.org/abs/2310.07956.

[9] de Oliveira Barbosa JM, Faragau AB, van Dalen KN, Steenbergen MJ. Modelling ballast via a non-linear lattice to assess its compaction behaviour at railway transition zones. J Sound Vib 2022;530:116942.

[10] Jain A, Metrikine A, Steenbergen M, van Dalen K. Dynamic amplifications in railway transition zones: investigation of key phenomena. J Phys: Conf Ser, IOP Publishing 2023.

[11] Jain A, van Dalen K, Metrikine A, Faragau A, Steenbergen M. Comparative analysis of the dynamic amplifications due to inhomogeneities at railway transition zones. In: Pombo J, editor. Proceedings of The Fifth International Conference on Railway Technology: Research, Development and Maintenance, Vol. CCC 1 of Civil-Comp Conferences. United Kingdom: Civil-Comp Press; 2023. https://doi.org/10.4203/ccc.1.19.1.

[12] Shan Y, Shu Y, Zhou S. Finite-infinite element coupled analysis on the influence of material parameters on the dynamic properties of transition zones. Constr Build Mater 2017;148:548–58. https://doi.org/10.1016/j.conbuildmat.2017.05.071.

[13] Shan Y, Li X, Zhou S. Multi-objective optimisation methodology for stiffness combination design of bridge-embankment transition zones in high-speed railways. Comput Geotech 2023;155:105242. https://doi.org/10.1016/j.compgeo.2022.105242.

[14] Varandas J, Hölscher P, Silva M. Three-dimensional track-ballast interaction model for the study of a culvert transition. Soil Dynam Earthquake Eng 2016;89:116–27. https://doi.org/10.1016/j.soildyn.2016.07.013.

[15] Ognibene G, Powrie W, Pen LL, Harkness J. Analysis of a bridge approach: long-term behaviour from short-term response. In: 15th Railway Engineering Conference, Edinburgh, U.K; 2019. p. 1–15.

[16] Heydari-Noghabi H, Zakeri J, Esmaeili M, Varandas J. Field study using additional rails and an approach slab as a transition zone from slab track to the ballasted track. Proc Inst Mech Eng, Part F: J Rail Rapid Transit 2017;232(4):970–8. https://doi.org/10.1177/0954409717708527.

[17] Coelho BZ, Hicks MA. Numerical analysis of railway transition zones in soft soil. Proc Inst Mech Eng, Part F: J Rail Rapid Transit 2015;230(6):1601–13. https://doi.org/10.1177/0954409715605864.

[18] Paixão A, Fortunato E, Calçada R. A numerical study on the influence of backfill settlements in the train/track interaction at transition zones to railway bridges. Proc Inst Mech Eng, Part F: J Rail Rapid Transit 2015;230(3):866–78. https://doi.org/10.1177/0954409715573289.

[19] Paixão A, Fortunato E, Calçada R. Design and construction of backfills for railway track transition zones. Proc Inst Mech Eng, Part F: J Rail Rapid Transit 2013;229(1):58–70. https://doi.org/10.1177/0954409713499016.

[20] Palomo ML, Martínez JHA, Arnoa AZ, Medina JJC. Structural and vibration performance in different scenarios of a prefabricated wedge for railway transition zones. J Vib Eng Technol 2021;9(7):1657–68. https://doi.org/10.1007/s42417-021-00319-5.

[21] Ribeiro CA, Calçada R, Delgado R. Calibration and experimental validation of a dynamic model of the train-track system at a culvert transition zone. Struct Infrastruct Eng 2017;14(5):604–18. https://doi.org/10.1080/15732479.2017.1380674.

[22] Zhang L, Jiang X, Li Z, Yang Z, Liu G, Dong Z, Qiu Y. Influence of the attenuation of subgrade elastic modulus caused by precipitation on ballasted track structure. Constr Build Mater 2022;352:128971. https://doi.org/10.1016/j.conbuildmat.2022.128971.

[23] Cai X, Liang Y, Xin T, Ma C, Wang H. Assessing the effects of subgrade frost heave on vehicle dynamic behaviors on high-speed railway. Cold Reg Sci Technol 2019;158:95–105. https://doi.org/10.1016/j.coldregions.2018.11.009.

[24] Wang H, Silvast M, Markine V, Wiljanen B. Analysis of the dynamic wheel loads in railway transition zones considering the moisture condition of the ballast and subballast. Appl Sci 2017;7(12):1208. https://doi.org/10.3390/app7121208.

[25] Gallego I, Muñoz J, Rivas A, Sánchez-Cambronero S. Vertical track stiffness as a new parameter involved in designing high-speed railway infrastructure. J Transport Eng 2011;137(12):971–9. https://doi.org/10.1061/(ASCE)TE.1943-5436.0000288.

[26] Jain A, Metrikine AV, Steenbergen MJMM, van Dalen KN. Railway transition zones: evaluation of existing transition structures and a newly proposed transition structure. Int J Rail Transportat 2023:1–21. https://doi.org/10.1080/23248378.2023.2272668.

[27] A. Fărăgău, A. Jain, J. de Oliveira Barbosa, A. Metrikine, K. van Dalen, Auxiliary rails as a mitigation measure for degradation in transition zones, in: J. Pombo (Ed.), Proceedings of The Fifth International Conference on Railway Technology: Research, Development and Maintenance, Vol. CCC 1 of Civil-Comp Conferences, Civil-Comp Press, United Kingdom, 2023. doi:10.4203/ccc.1.19.4.

[28] Marelli S, Sudret B. Uqlab: A framework for uncertainty quantification in matlab, in: Vulnerability, Uncertainty, and Risk, American Society of Civil Engineers; 2014. doi:10.1061/9780784413609.257. doi: 10.1061/9780784413609.257.

[29] ABAQUS/Standard User's Manual, Version 6.9, Dassault Systèmes Simulia Corp, United States.

[30] Abaqus Theory Manual (V6.6), Dassault Systèmes Simulia Corp, United States. https://classes.engineering.wustl.edu/2009/spring/mase5513/abaqus/docs/v6.6/books/stm/default.htm?startat=ch01s05ath12.html.

[31] R.A.F. da Silva, Viability and Applicability of Simplified Models for the Dynamic Analysis of Ballasted Railway Tracks (2017). http://hdl.handle.net/10362/21663.

[32] Sudret B. Global sensitivity analysis using polynomial chaos expansions. Reliab Eng Syst Saf 2008;93(7):964–79. https://doi.org/10.1016/j.ress.2007.04.002.

[33] M. Mohammadi, A. Mosleh, M. Razzaghi, P.A. Costa, R. Calçada, Stochastic analysis of railway embankment with uncertain soil parameters using polynomial chaos expansion, Structure and Infrastructure Engineeringdoi:10.1080/15732479.2022.2033277.

[34] Marelli S, Sudret B. Uqlab: A framework for uncertainty quantification in matlab. Vulnerability, Uncertainty, and Risk 2014:2554–63. https://doi.org/10.1061/9780784413609.257. URL https://ascelibrary.org/doi/abs/10.1061/9780784413609.257.

[35] Blatman G. Adaptive sparse polynomial chaos expansion for uncertainty propagation and sensitivity analysis. Ph.D. thesis. Clermont: Blaise Pascal University; 2009.

[36] Blatman G, Sudret B. Adaptive sparse polynomial chaos expansion based on least angle regression. J Comput Phys 2011;230(6):2345–67. https://doi.org/10.1016/j.jcp.2010.12.021.

[37] Huber F. A Logical Introduction to Probability and Induction. Oxford University Press; 2018.

[38] Hogg RV, Craig AT. Introduction to Mathematical Statistics 1959. URL https://api.semanticscholar.org/CorpusID:122755063.

[39] Ewing WM, Jardetzky WS, Press F. Elastic Waves in Layered Media. McGraw-Hill Publishing Co.; 1957.

[40] Achenbach JD. Wave Propagation in Elastic Solids. Applied Mathematics and Mechanics Series. North-Holland Publishing Company; 1973.